

Fragment-Based Drug Discovery Applied to Hsp90. Discovery of Two Lead Series with High Ligand Efficiency[†]

Christopher W. Murray,* Maria G. Carr, Owen Callaghan, Gianni Chessari, Miles Congreve, Suzanna Cowan, Joseph E. Coyle, Robert Downham, Eva Figueroa, Martyn Frederickson, Brent Graham, Rachel McMenamin, M. Alistair O'Brien, Sahil Patel, Theresa R. Phillips, Glyn Williams, Andrew J. Woodhead, and Alison J.-A. Woolford

Astex Therapeutics, Ltd., 436 Cambridge Science Park, Milton Road, Cambridge CB4 0QA, U.K.

Received January 15, 2010

Inhibitors of the chaperone Hsp90 are potentially useful as chemotherapeutic agents in cancer. This paper describes an application of fragment screening to Hsp90 using a combination of NMR and high throughput X-ray crystallography. The screening identified an aminopyrimidine with affinity in the high micromolar range and subsequent structure-based design allowed its optimization into a low nanomolar series with good ligand efficiency. A phenolic chemotype was also identified in fragment screening and was found to bind with affinity close to 1 mM. This fragment was optimized using structure based design into a resorcinol lead which has subnanomolar affinity for Hsp90, excellent cell potency, and good ligand efficiency. This fragment to lead campaign improved affinity for Hsp90 by over 100000-fold when the addition of only six heavy atoms. The companion paper (DOI: 10.1021/jm100060b) describes how the resorcinol lead was optimized into a compound that is now in clinical trials for the treatment of cancer.

Introduction

Molecular chaperones are proteins that play a role in the conformational stability, maturation, and function of other substrate proteins, which are known as clients.¹ Heat shock protein 90 (Hsp90⁶) is a molecular chaperone, and many of its clients are oncology targets that are known to play critical roles in cancer progression.^{2,3} In fact it has been argued that interference with Hsp90 and its associated clients can allow the simultaneous targeting of the hallmarks of cancer, i.e., self-sufficiency in growth signals, insensitivity to antigrowth and apoptotic signaling, angiogenesis, limitless replicative potential, invasion, and metastasis.^{2,4,5} It was initially thought that inhibition of the Hsp90 chaperone cycle would lead to unacceptable toxicities due to the ubiquitous expression of Hsp90 in normal cells.⁶ However, later work has shown that Hsp90 inhibition can lead to reasonably specific inhibition in cancer cells because Hsp90 is present in an activated form.^{6,7} Additionally, the preclinical and, more recently, clinical activity of geldanamycin-based inhibitors has indicated the potential utility of Hsp90 inhibitors.^{2,8}

The chaperone cycle of Hsp90 involves the turnover of ATP to ADP through an ATPase activity associated with the N-terminal domain of Hsp90.⁹ The ATP binding site has been characterized crystallographically, and the binding modes of a

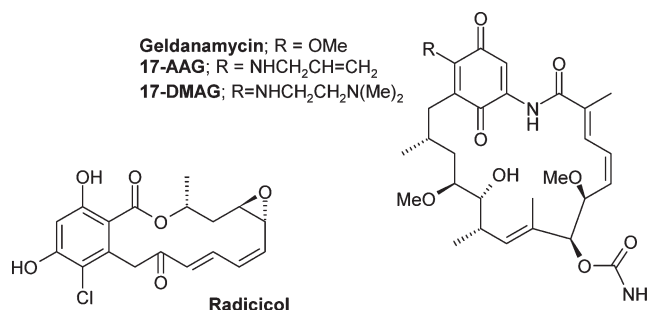


Figure 1. Natural product derived inhibitors of Hsp90. Note that 17-DMAG, 17AAG, and the quinol form of 17AAG (i.e., IPI-504) have been progressed into clinical trials.

number of Hsp90 inhibitors have been determined.⁹ It has also been demonstrated that inhibition leads directly to the down-regulation of client proteins and antiproliferative activity.¹⁰ At the start of our Hsp90 program the most advanced Hsp90 inhibitors were derived from natural products^{11–15} (see Figure 1) and our aim was to use fragment-based drug discovery (FBDD) to derive a synthetic inhibitor of Hsp90 with improved pharmaceutical properties. There are now a number of reviews describing synthetic Hsp90 inhibitors,^{16–19} and Figure 2 gives structures of compounds currently in clinical development.^{20–25}

Fragment-based drug discovery (FBDD) is gathering momentum in the pharmaceutical industry, and a number of clinical candidates or advanced leads have been identified via the approach.^{26–34} A recent review has listed the key concepts that lie behind the rise in FBDD, and we recapitulate these to provide some background to the field. The first concept is that inappropriate physical properties are thought to be a major driver for attrition in drug development,^{35–38} and there is

[†]Coordinates for the Hsp90 complexes with compounds **1**, **3**, **4**, **2 + 4**, **6**, **14**, **21**, **24**, and **31** have been deposited in the Protein Data Bank (PDB) under accession codes 2xdk, 2xdl, 2xdx, 2xds, 2xdx, 2xhr, 2xht, 2xhx, and 2xab, respectively, together with the corresponding structure factor files.

*To whom correspondence should be addressed. Phone: +44 (0)1223 226228. Fax +44 (0)1223 226201. E-mail: c.murray@astex-therapeutics.com.

^aAbbreviations: CDK4, cyclin dependent kinase 4; FBDD, fragment-based drug discovery; Hsp70, heat shock protein 70; Hsp90, heat shock protein 90; ITC, isothermal titration calorimetry; LE, ligand efficiency; PDB, Protein Data Bank.

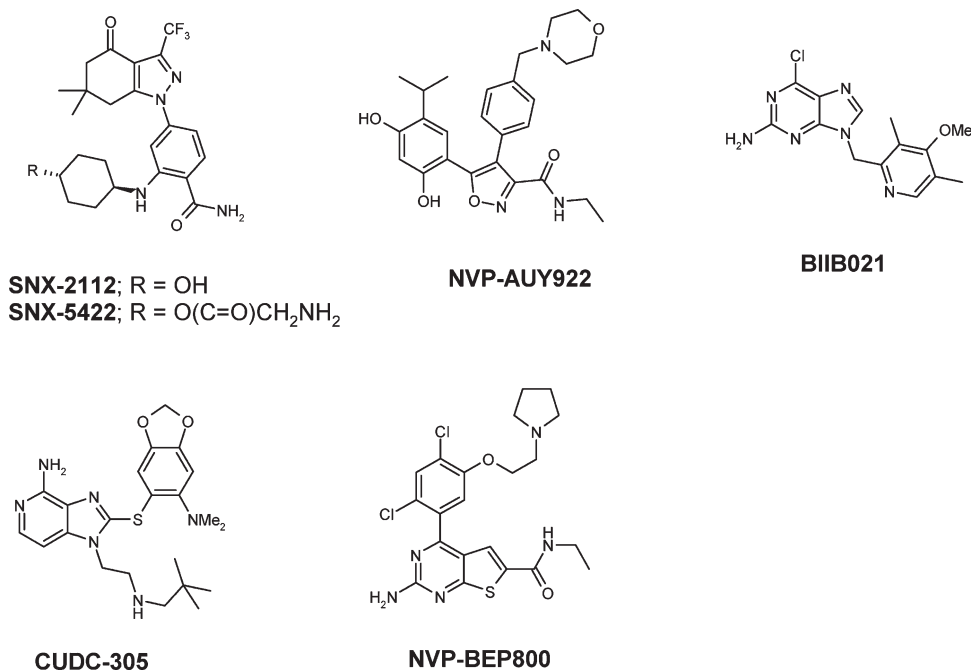


Figure 2. Synthetic inhibitors of Hsp90 currently in clinical trials.

therefore a need to explore alternative methods, such as FBDD, that might deliver candidates with improved physical properties. It will take many FBDD applications across many different targets before progress in this regard can be properly assessed. Fragments are compounds of low molecular weight (usually 100–250 Da) and typically have low binding affinities ($> 100 \mu\text{M}$), but a second key concept is that fragments form high-quality interactions despite their weak potency and therefore can provide attractive starting points for medicinal chemistry. In our application we will show that this is true for Hsp90, although no single application can be used to assess a general point. A third concept important to FBDD is that ligand efficiency (LE)^{39,40} can be used to track the potency of fragment hits during lead identification and to assess whether gains in potency are significant enough to justify increases in molecular size. LE can be defined as

$$\text{LE} = \frac{-\Delta G}{\text{HAC}} = \frac{-RT \ln(K_d)}{\text{HAC}}$$

where ΔG is the free energy of binding of the ligand for a specific protein, HAC is the number of heavy atoms in the ligand, and K_d represents the dissociation constant for the protein–ligand complex (IC_{50} is often used instead of K_d). This paper illustrates the use of LE during fragment optimization against Hsp90 but also illustrates that LE is not the only criteria that should be used to select which fragments to optimize. The fourth concept behind FBDD is that relatively small libraries of fragments are required to sample chemical space and some elegant models have been described in the literature to illustrate this behavior.^{41,42} Here no analysis of the sampling advantages of fragments is presented but our application does show the identification of two distinct chemical leads for Hsp90 derived from screening a library of only 1600 fragments.

The motivation of this paper is to describe how biophysical methods (NMR and X-ray crystallography) have been used to perform fragment screening against the N-terminal domain of Hsp90. The paper shows how two fragment hits were then

efficiently optimized into potent lead series. The results are discussed together with any learning points that are relevant to either Hsp90 inhibition or FBDD. A companion paper (DOI: 10.1021/jm100060b) describes how one of these leads was optimized into an Hsp90 inhibitor that is currently in clinical trials for the treatment of cancer.

Results and Discussion

Fragment Screening for Hsp90. Approximately 1600 compounds from our fragment library⁴³ were screened in cocktails using ligand observed NMR via water LOGSY.⁴⁴ Compounds showing a medium or strong LOGSY signal (as defined in the Experimental Section) were further characterized according to competition for the nucleotide site. NMR screening was carried out in the presence of a low concentration of the product, ADP, which binds weakly to the ATP-ase domain of Hsp90 under the screening conditions. Cocktails that contained fragments that bound to the nucleotide site of the target could be identified immediately by observing the displacement of ADP, estimated from the reduction in its own LOGSY signal. Further information on the affinity of the fragment at this site was obtained in a second step by adding 5 mM Mg^{2+} to the screening solution. This increases the affinity of ADP for the active site and leads to the displacement of more weakly bound fragments. A total of 125 fragments were progressed into crystallography after analysis of the NMR data and a consideration of chemical diversity. Of these compounds 26 fragment crystal structures were obtained, spanning a variety of chemotypes. The chemical structures for four of the validated hits are shown in Figure 3.

All affinities given in this paper are dissociation constants determined by isothermal titration calorimetry (ITC) (see Experimental Section for more details and for ITC values obtained with reference compounds). All ligand efficiencies are calculated directly from the ITC dissociation constants and have units of kcal per heavy atom.

Compound **1** has a measured affinity of $250\ \mu\text{M}$ and ligand efficiency of 0.38. The binding mode for this fragment is given in Figure 4a. The molecule lies in a deep pocket where it forms an extensive network of hydrogen bonds with the side chain of Asp93 and four crystallographically observed water molecules trapped at the bottom of the pocket. The aminopyrimidine interactions are similar to those observed with the adenine ring in the ADP complex (Figure 4b). Interestingly, compound **1** is twisted about the bond connecting the pyridine to the pyrimidine. As discussed in more detail below, this is not the most stable geometry in the absence

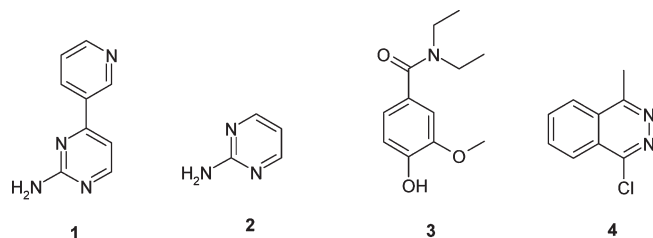


Figure 3. Chemical structures of four validated hits identified by fragment screening against Hsp90.

of the protein, so it should be possible to improve the affinity through stabilization of the protein bound conformation. Furthermore, compound **1** is doing a poor job of filling the proximal lipophilic pocket lined by the lipophilic side chains of Met98, Leu107, Phe138, Val150, and Val186 (see Figure 4c), and so improved hydrophobic fit in this region may be advantageous.

Compound **2** is an example of an even simpler aminopyrimidine that was observed to bind crystallographically even though it has very weak affinity ($> 1\ \text{mM}$). Figure 4d displays the $F_o - F_c$ unrefined electron density map for this complex, and despite its small size and weak affinity, the aminopyrimidine can be unambiguously placed within the map together with a number of density peaks associated with tightly bound water molecules. Comparison of Figure 4d with Figure 4b shows that the simpler aminopyrimidine forms the same contacts as compound **1**.

Compound **3** has an affinity of $790\ \mu\text{M}$ and a ligand efficiency (LE) of 0.26 and is a known drug (ethamivan) with respiratory stimulant activity.⁴⁵ Figure 5a shows the binding mode in a similar frame of reference to compound **1** in Figure 4b. It can be seen that the phenolic OH of compound **3** displaces one of the water molecules observed

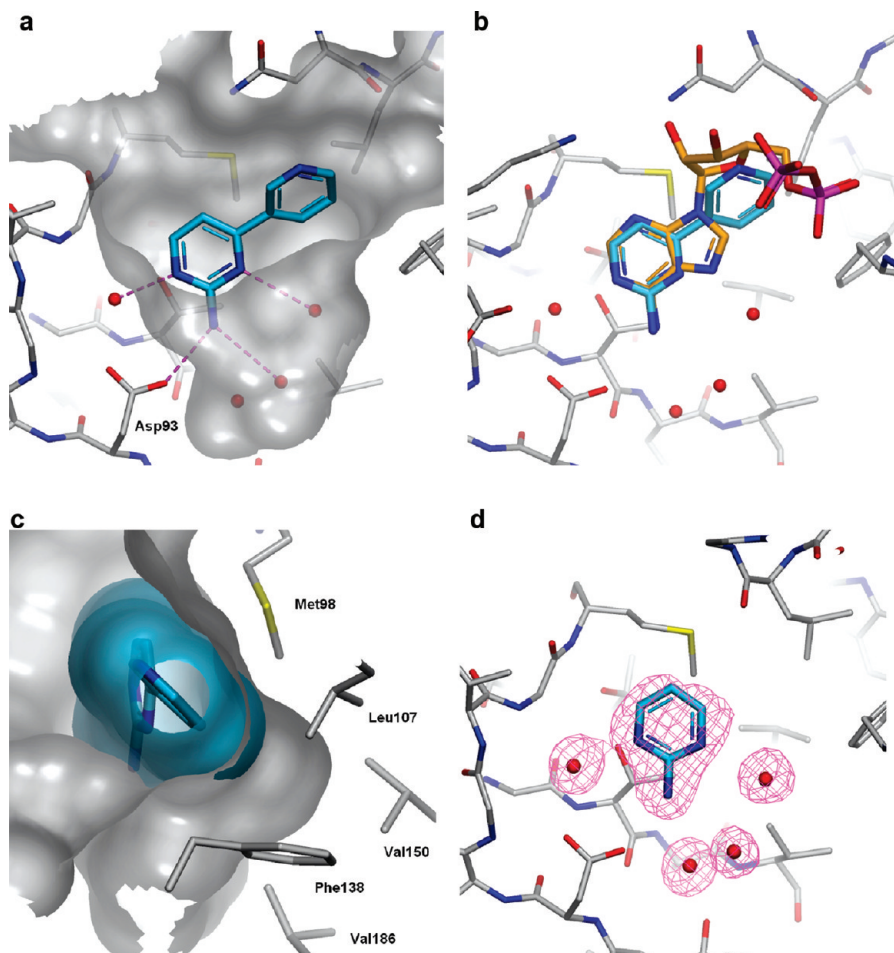


Figure 4. Binding mode of aminopyrimidine fragments in Hsp90. (a) Compound **1** forms multiple hydrogen bonds with water molecules and the side chain of Asp93 at the bottom of the ATP binding site. The bond between the two aromatic rings is heavily twisted. (b) The crystallographic overlays of compound **1** and ADP illustrate the conserved nature of the interactions. (c) Protein surface in gray and the ligand surface in cyan for the complex of Hsp90 and compound **1**. For clarity the only protein residues shown are the residues that line the proximal lipophilic pocket (Met98, Leu107, Phe138, Val150, and Val186). The bulge on the middle-right-hand side of the protein surface represents the proximal lipophilic pocket. It is poorly filled by the ligand surface and is not occupied by water molecules. (d) $F_o - F_c$ electron density map contoured at 4σ for compound **2**. The view has been clipped to aid visualization.

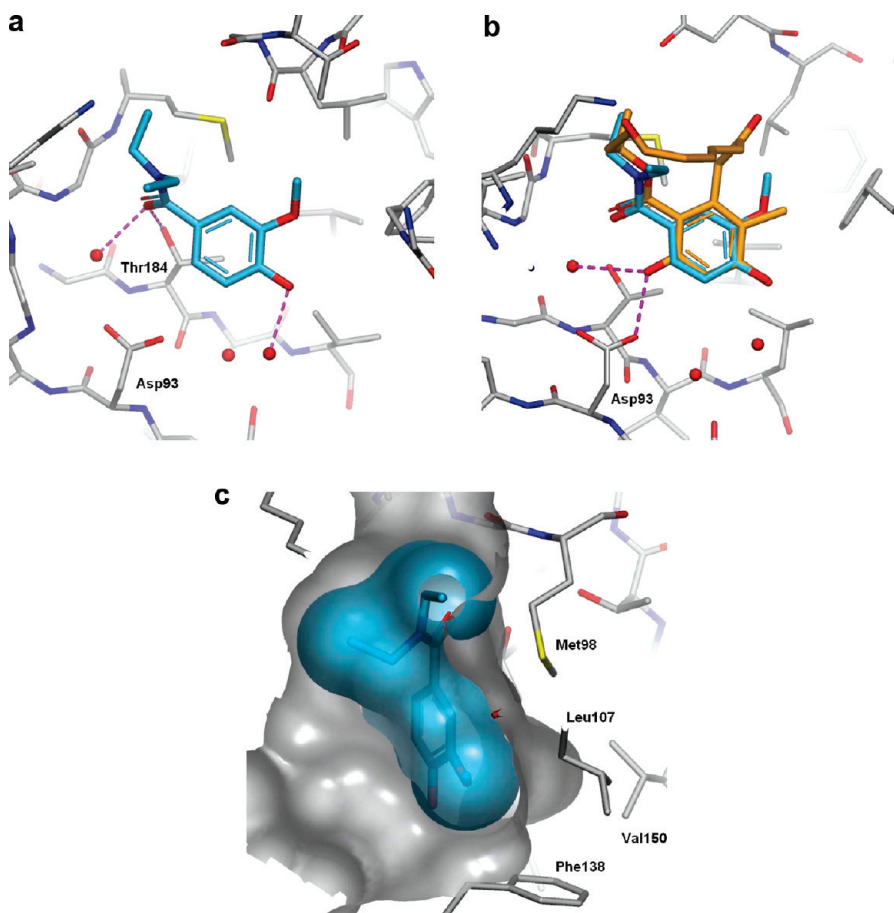


Figure 5. Binding mode of phenol fragment **3** in Hsp90. (a) Compound **3** displaces one of the water molecules (compare with Figure 4a and Figure 4b) and forms hydrogen bonds with two of the conserved water molecules at the bottom of the ATP binding site. (b) Crystallographic overlay of compound **3** with the natural product radicicol (PDB code 1BGQ). The additional hydroxyl group in radicicol makes a direct hydrogen bond with Asp93 and with a conserved water molecule. (c) Protein surface in gray and the ligand surface in cyan for the complex of Hsp90 and compound **3**. For clarity, the only protein residues shown are the residues that line the proximal lipophilic pocket (Met98, Leu107, Phe138, Val150, and Val186). The bulge on the lower-right-hand side of the protein surface represents the proximal lipophilic pocket. It is poorly filled by the ligand surface and is not occupied by water molecules.

in the pyrimidine/purine structures and forms a hydrogen bond with one of the remaining conserved water molecules. The carbonyl of compound **3** forms a hydrogen bond with the side chain of Thr184 and with a conserved water molecule (mediating to Asp93), but there is no direct hydrogen bond to Asp93. Despite its poor ligand efficiency, the crystallographic binding mode offered the promise of a fast fragment optimization campaign. Superimposition of the structure on the yeast Hsp90 complex with the natural product, radicicol⁴⁶ (Figure 5b) indicated that conversion of the phenol to the corresponding resorcinol would allow the formation of a direct hydrogen bond to Asp93 and an additional water-mediated hydrogen bond. These interactions are common to all known active site inhibitors of Hsp90, and we reasoned that this would yield a large increase in affinity and ligand efficiency. The protein–ligand complex also suggested another potential route to fragment optimization. The methoxy group of fragment **3** does not properly fill the proximal lipophilic pocket defined by the side chains of Met98, Leu107, Phe138, Val150, and Val186 (Figure 5c), and its replacement with other substituents might also be beneficial.

Compound **4** has an affinity > 1 mM with an LE < 0.34, and it binds in a lipophilic pocket away from Asp93. The formation of the pocket is driven by the substantial

rearrangement of residues Ile110–Gly114 which become the central portion of a long helix. Figure 6a illustrates this change in protein secondary structure by superimposing the structures for fragments **2** and **4**. The conformational movement has previously been observed with larger compounds in Hsp90⁴⁷ and has also been reported with fragments, although no X-ray structures of fragments have been disclosed.^{48,49} Other conformations for this mobile region were also observed during our Hsp90 project, but this one is notable because it opens up a large lipophilic pocket that can be exploited in drug design. Fragment **4** makes only lipophilic interactions with the induced pocket formed by the side chains of Leu107, Phe 138, Tyr139, and Trp162. Figure 6b shows the result of an experiment where compounds **2** and **4** were cosoaked into Hsp90 that resulted in both compounds being observed to bind at the same time. The fragment binding modes in the individual fragment complexes are identical to the binding modes observed in the cosoak. Superimposition of the cosoak structure of **2** + **4** with other structures indicates that fragment **4** occupies a region that is filled by the side chain of Leu107 in the fragment **2** complex. A valid design approach would be to attempt to link together fragments **2** and **4**, but the rest of this paper focuses on a fragment growth strategy starting from either compound **1** or compound **3**.

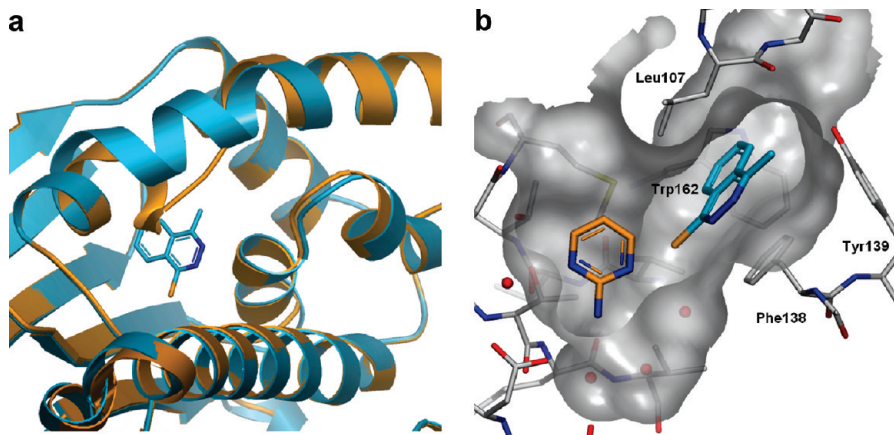
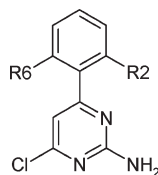


Figure 6. (a) Crystallographic complex of Hsp90 with **4** (in cyan) superimposed on the complex with **2** (in orange). The proteins are displayed in schematic form. The upper left helix is continuous with fragment **4** but is interrupted in a more typical complex with fragment **2**. This substantial conformational movement is induced by the binding of fragment **4**. (b) Binding mode of fragments **2** and **4** when cosoaked with Hsp90. Fragment **4** binds in an induced, slot-shaped, hydrophobic pocket flanked by the lipophilic side chains of Leu107, Phe138, Tyr139, and Trp162.

Table 1. Substitution with Small Groups at R1 and R2 Enhances Potency of the Aminopyrimidines



compd	R2	R6	ITC (μM)	LE	cell IC ₅₀ (μM)
1 ^a			250	0.38	
5	H	H	2	0.56	
6	OMe	H	0.35	0.55	
7	OMe	OMe	0.068	0.54	7.9
8	Cl	OMe	0.036	0.6	6.4
9	Cl	H	0.083	0.64	18

^aThe chemical structure for **1** is shown in Figure 3

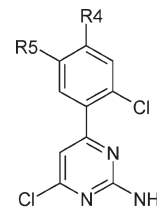
Optimization of Aminopyrimidines Starting from Fragment 1.

Tables 1 and 2 give data and chemical structures for the aminopyrimidines covered in this section. The tables give dissociation constants obtained with isothermal titration calorimetry, and the cell IC₅₀ values reflect the inhibition of HCT116 cell proliferation.

The crystal structure of Hsp90 with compound **1** shows that the fragment is twisted about the bond connecting the pyridine to the pyrimidine (torsion angle of 47.6°) despite the presence of an aromatic nitrogen atom ortho to this bond. Small molecule crystal structures⁵⁰ and the torsion profile reported in Figure 7a both suggest that the optimal geometry for such ring systems is close to planarity, so it should be possible to improve the affinity through stabilization of the protein bound conformation.

Optimisation of fragment **1** began with virtual screening of close analogues and resulted in the purchase of the simple chloro analogue, compound **5**, that showed an improvement in affinity of approximately 100-fold. Initial synthesis focused on analogues of compound **5** with the aim of stabilizing the twist observed in the X-ray structure and filling the proximal lipophilic pocket that is formed by lipophilic side chains of Met98, Leu107, Phe138, Val 150, and Val186. From the crystal structure of fragment **1**, the elegant way

Table 2. Further SAR around the Upper Phenyl Ring of the Aminopyrimidines



Compound	R4	R5	ITC (μM)	LE	Cell IC ₅₀ (μM)
10	Cl	H	0.012	0.68	4.1
11	H	OMe	0.048	0.59	7.9
12	Cl	OMe	0.0063	0.62	1.8
13	OMe	H	0.028	0.61	
14	Cl		0.0048	0.45	1.9

to achieve this was to substitute the upper phenyl ring at the 2 and/or 6 position with small groups (Figure 4c).

The first compound synthesized was the 2-methoxy analogue **6**, which showed a 5-fold improvement in affinity and a crystal structure showed that the compound bound in the desired conformation (coordinates have been deposited with the PDB). However, there was a concern that this was still not the most favored ligand conformation. The torsion energy profile of **6** indicated that the methoxy group might prefer to sit on the other side of ring to avoid a clash with the pyrimidine nitrogen and that the conformation observed in the crystal structure (torsion angle of 48.1°) is a local minimum which is ~3 kcal/mol higher in energy than the global minimum (see Figure 7b). This reasoning was supported by further SAR. For example, the 2,6-dimethoxy compound **7** offered a further 5-fold improvement over compound **6** despite the fact that the second methoxy group made no direct contact with the enzyme. Additionally the 2-chloro compound **9** was significantly more potent than compound **5**. The torsion profile of **9** suggests that mutating the methoxy group with a chloro reduces to only ~1 kcal/mol the

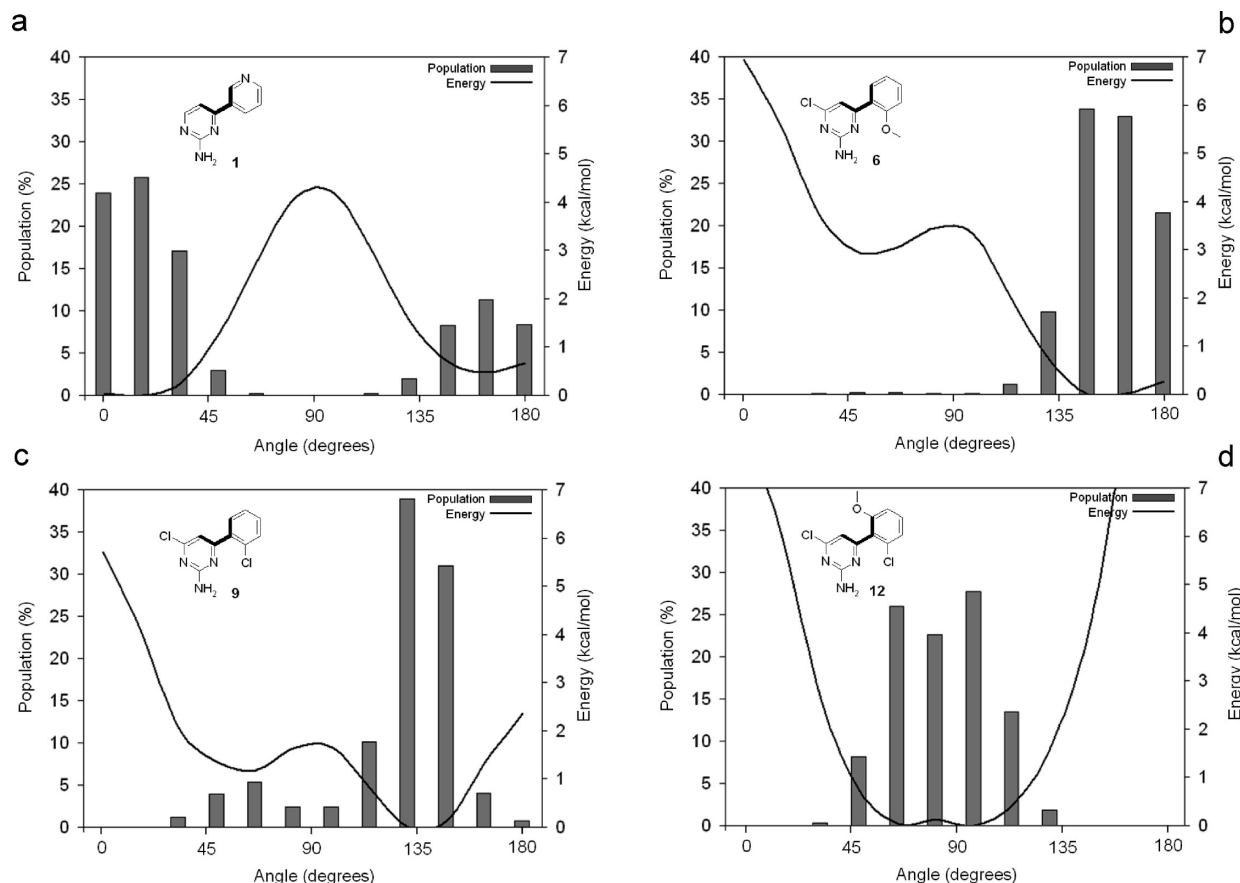


Figure 7. Energy profiles and population histograms of compounds **1**, **6**, **9**, and **12**. The continuous line on the plots gives the relative potential energy calculated by B3LYP/6-311G* as a function of the torsion angle for each structure. The scale on the right-hand side of the plots gives the relative potential energies in kcal/mol. The relative population of each torsion angle in the gas phase is estimated from the Boltzmann distribution and is shown as a histogram with the percentage population shown on the left-hand scale in the plot. The torsional angle being considered is highlighted in bold in the chemical structures.

difference in energy between local and the global minimum (see Figure 7c). Finally, the 2-chloro-6-methoxy compound **8** only marginally improves upon this affinity and the torsional distribution for **8** shows that all conformations with a torsion angle between 60° and 110° are isoenergetic (see Figure 7d). Generally the calculated torsion distributions provided useful predictions of the activity changes observed in the initial round of synthesis.

Compound **9** was the most ligand efficient molecule from the initial synthesis iteration and was chosen as the basis for the next iteration. Crystal structures on this series indicated that further substitution of the upper phenyl ring with small groups at the 4-position might facilitate additional lipophilic interactions with the enzyme. Methoxy or chlorine substitution significantly increased affinity with compound **10** having an affinity of 12 nM and very high ligand efficiency (0.68).

Further work on this series was focused on trying to improve the physical properties and the cell activity of compound **10**. The structural work suggested that substitution at the 5 position of the upper phenyl ring might be used to allow the introduction of solubilizing groups with the aim of improving cell activity. The 5-methoxy group **12** offered a 2-fold improvement in measured potency (although note that the error in ITC determination is approximately 2-fold). It also served as a growth point for the introduction of solubilizing groups such as the morpholine group exemplified in compound **14**. This compound has low micromolar

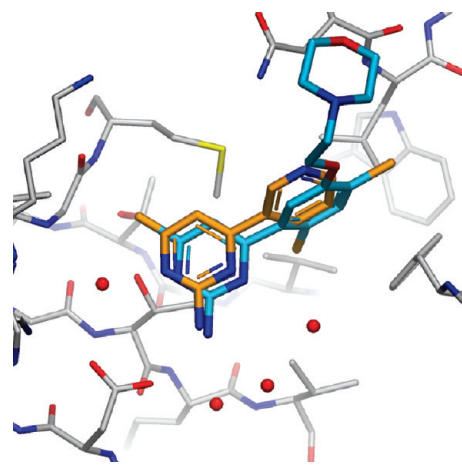
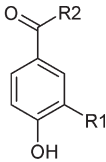
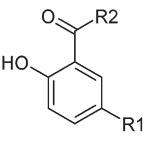
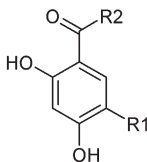


Figure 8. Crystallographic complex of Hsp90 with **14** (in cyan) superimposed on the complex with **1** (in orange). The original binding mode of the fragment is maintained in the final complex.

activity in the cell assay and may be a potential lead molecule versus Hsp90. The crystal structure of compound **14** is shown in Figure 8 and is in good agreement with the design hypotheses; the superimposition in Figure 8 also illustrates that the final molecule forms the same interactions as the initial starting fragment.

Optimization of Phenols Starting from Fragment 3. The binding mode of fragment **3** indicated that the methoxy

Table 3. Optimization of the Phenol Series

										
		4-OH formula	2-OH formula	2,4-OH formula						
Compound	Formula	R1	R2	ITC (μ M)	LE	Cell IC ₅₀ (μ M)				
3	4-OH	OMe		790	0.26					
15	4-OH	Cl		1130	0.27					
16	4-OH	Et		45	0.37					
17	4-OH	iPr		7	0.41					
18	4-OH	tBu		8.6	0.38					
19	2-OH	iPr		51	0.34					
20	2-OH	tBu		134	0.29					
21	4-OH	tBu		1.1	0.43	22				
22	4-OH	tBu		2.3	0.38					
23	4-OH	tBu		2.5	0.35					
24	4-OH	tBu		0.25	0.41					
25	4-OH	tBu		2.5	0.31	8.3				
26	4-OH	tBu		0.4	0.38	7.9				
27	4-OH	iPr		0.47	0.48	71				
28	4-OH	iPr		0.068	0.47	17				
29	4-OH	iPr		0.128	0.43	15				
30	2,4-OH	iPr		0.011	0.57	0.14				
31	2,4-OH	iPr		0.00054	0.57	0.031				

group could be replaced by substituents which filled the proximal lipophilic pocket. Chloro (**15**), ethyl (**16**), isopropyl (**17**), and *tert*-butyl (**18**) analogues were initially synthesized (Table 3). The chloro group showed no improvement, while the ethyl group showed a 20-fold improvement. The best groups were *tert*-butyl and isopropyl, which were approximately 100-fold more potent. The superior filling of the proximal lipophilic pocket was confirmed by crystallography on compound **18** (data not shown).

Radicicol (Figure 1) is a resorcinol and contains an additional OH group at the 2-position compared with 4-OH

substituted compounds. Given that this 2-OH group in radicicol forms a direct hydrogen bond to Asp93, we were interested to see whether a phenol based on this substitution pattern would have superior affinity. Compounds **19** and **20** were prepared, but these were about 10-fold less potent than the corresponding 4-OH substituted compounds. This implied that the 4-OH group must be a significant contributor to the affinity of the series, presumably derived from the favorable displacement of a mediating water molecule observed in the ADP and pyrimidine complexes (compare Figure 5a with Figure 4b).

The next synthetic iteration investigated a selection of amides to replace the diethylamide in compound **18**. The X-ray structure indicated the importance of the carbonyl group which forms a direct hydrogen bond with the side chain of Thr184 and a strong water-mediated hydrogen bond with Asp93 (see Figure 5a). The torsion between the carbonyl and phenyl ring is highly twisted (61° in compound **18**), and the torsion is stabilized by the tertiary nature of the amide. The design therefore focused on tertiary amides, and modeling indicated that they would be directed toward the side chain of Lys58 which is well-defined in the electron density (Lys58 is visible in the upper-left-hand side of Figure 5a and Figure 5b). The first design idea was to form a hydrogen bond with the amine on Lys58. Compounds **21**, **22**, and **23** are representative of a small number of compounds that test this idea, and all these compounds offer an affinity improvement of about 50-fold, with compound **21** being the best and most ligand efficient. Figure 9a shows the crystal structure of **21** and confirms the formation of a good hydrogen bond between the morpholine oxygen and Lys58. The second design idea centered on trying to displace the side chain of Lys58 with larger tertiary amides that might then form good lipophilic interactions with the protein. The lysine side chain itself forms no specific contacts with the enzyme and seemed a plausible candidate for displacement despite its relatively clear positioning in the electron density. Compounds **24**, **25**, and **26** are representative molecules, and the isoindoline **24** delivered an affinity improvement of several-hundred-fold. Figure 9b shows the crystal structure of **24** where it can be seen that the side chain of Lys58 has indeed moved away and forms a salt bridge with Glu62. The space formerly occupied by Lys58 accommodates the phenyl ring of the isoindoline which forms good lipophilic contact with Ala55, Lys58, and Ile96. Interestingly and perhaps surprisingly, it was therefore possible to increase potency significantly by either forming a direct hydrogen bond with the side chain of Lys58 or displacing the side chain with lipophilic groups. The best amides from the previous synthesis iteration were then combined with the isopropyl group. This yielded a further 2- to 4-fold improvement for compounds **27**, **28**, and **29** (the error in the ITC measurement is about 2-fold, so this probably represents a real improvement). The change to the isopropyl group also reduced the lipophilicity by about 0.5 unit.

The final change was to convert the best phenols into resorcinols driven by the similarity of the binding mode of our compounds to the natural product radicicol (Figure 5b). The morpholine compound **30** is 40-fold more potent than the corresponding 4-OH compound **27** and has an improved cell activity of 140 nM. The isoindoline resorcinol **31** shows subnanomolar affinity, excellent ligand efficiency, and good cell activity (31 nM). For compounds **30** and **31**, the additional hydroxyl group gave large improvements in affinity

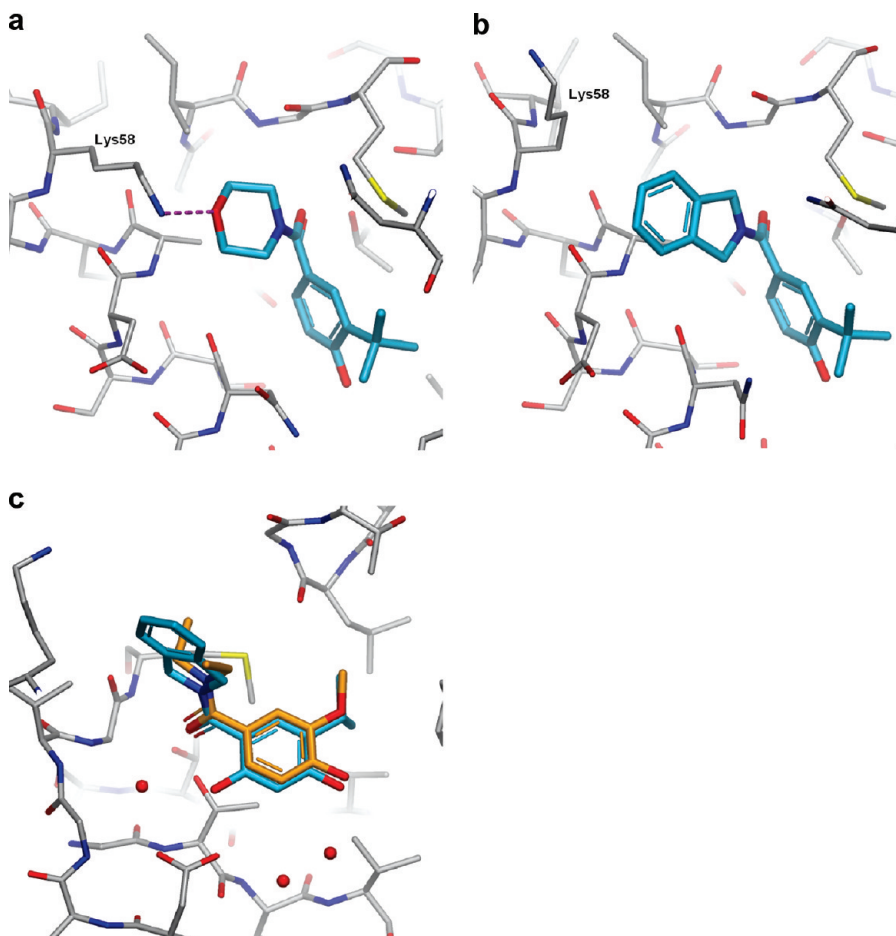


Figure 9. Development of the lead compound from the phenol series. (a) Experimental binding mode of compound **21** illustrating the formation of a new hydrogen bond with the side chain of Lys58. (b) Experimental binding mode of compound **24** in which Lys58 is displaced by the isoindoline group. In its new position, the side chain of Lys58 forms a salt bridge with Glu62. (c) Experimental binding mode of lead molecule **31** (in cyan) superimposed on the original fragment **3** (in orange).

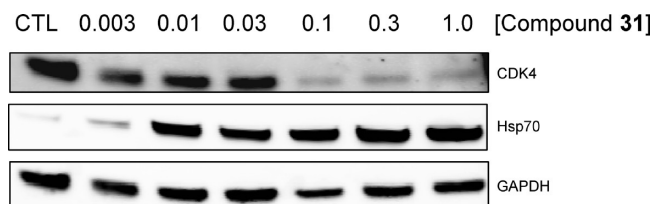


Figure 10. Effects of different concentrations of **31** on the levels of CDK4 and Hsp70 in HCT116 cells as determined by Western blot. Included as controls are the levels of GAPDH protein and the levels when no compound is added to HCT116 cells (shown as CTL).

but also gave much better translation between the measured affinities and the cell activity (for reasons that were not established). Figure 9c gives the binding mode of compound **31** in Hsp90, and as anticipated, the additional hydroxyl group forms good hydrogen bonds with Asp93 and a mediating water molecule. The superimposition with the original fragment demonstrates that the binding mode was preserved during the fragment optimization campaign.

Figure 10 shows Western immunoblotting data for HCT116 cells treated with **31** and confirms that the compound has the anticipated molecular signature of an Hsp90 inhibitor;^{3,10} the client protein CDK4 is depleted, while the chaperone protein Hsp70 is induced. These effects occur at concentrations similar to the IC₅₀ for the inhibition of cell

proliferation in the HCT116 cells. Compound **31** was chosen as the lead compound, and further biological characterization of the series is described in the companion paper (DOI: 10.1021/jm100060b).

Discussion and Conclusion

We have applied the Pyramid screening technique to Hsp90 and exploited a close integration of ligand observed NMR screening and high throughput X-ray crystallography. We found it necessary to use a combination of cocrystallography and soaking into different crystal forms of Hsp90 in order to maximize the number of high quality X-ray structures obtained. From this process, 26 fragment structures were obtained during the screening phase of the project, and four of these fragments are disclosed in this paper. Perhaps most surprising were fragments such as **4** which bind to an induced lipophilic pocket and the successful cocrystallization of this fragment with 2-aminopyrimidine. Huth et al. have recently described a similar observation and detailed an NOE-based NMR structure determination for the tertiary arrangement of two fragments, one of which was a simple aminopyrimidine.⁴⁸

Choosing which fragments to work on is one of the parts of fragment based discovery that requires judgment. Ligand efficiency^{39,40} is one criterion that we have used extensively, but it is not the only factor. Here fragment **3** had relatively poor ligand efficiency (0.26) but its binding mode suggested a

number of design ideas for improvement, i.e., by converting the phenol into a resorcinol or by properly filling the proximal lipophilic pocket. Experience on a variety of projects has demonstrated that ligand efficiency can be improved where there is a clear and correctable deficiency in the binding mode of the fragment. However, if this cannot be rapidly achieved, it is usually better to terminate work on such a fragment. Similarly, although fragment **1** had better ligand efficiency (0.38), its crystal structure suggested a design strategy to improve potency, i.e., stabilizing the active conformation and filling the proximal lipophilic pocket. This emphasizes that the binding mode of the fragment and the attractiveness of the associated medicinal chemistry plan are important determinants in judging which fragments to pursue.

Subsequent to this work Brough et al. have disclosed a parallel virtual screening and fragment screening approach to Hsp90.²⁰ Aminopyrimidine based hits were identified by both approaches, and structure based drug design was used to hybridize hits from molecules with related binding modes. This approach successfully led to a clinical candidate. In our work, we have used virtual screening in a different manner to explore SAR around very close analogues of identified fragments. For example, the binding mode of fragment **3** was used to inform a virtual fragment screen culminating in the identification of fragment **5**. This more conservative approach may allow more control over the molecular size and ligand efficiency of the developing lead series. Virtual screening of designed compounds was also heavily used to prioritize synthesis during fragment optimization.

Relatively small libraries of compounds are required to perform fragment screening, and if researchers rely on commercially available compounds, it is likely that the same fragments will appear in fragment screening collections from different companies. This represents an emerging challenge for FBDD practitioners to improve the novelty of fragments in their libraries and to establish strategies for introducing novelty as molecules are optimized. Hsp90 is a good example on which to assess this because a large number of research groups have worked on this target and some of these groups have used FBDD. The work on aminopyrimidines by Brough et al. illustrates how novelty can be introduced through the fusion of a heterocycle onto an initial aminopyrimidine fragment.²⁰ Barker et al. identified aminopyrimidine fragments containing a semisaturated ring fused onto the aminopyrimidine and presumably attained novelty as a result.⁴⁹ We first described our aminopyrimidine series in a patent several years ago,⁵¹ and subsequently Huth et al. have described the development of a similar series using FBDD.⁴⁸ In the present work, the fragment screening and optimization approach are different, and the final compound shows activity in cells. Resorcinol compounds have been worked on by a number of groups.¹⁶ Both high throughput screening and fragment screening approaches were used in the development of NYP-AUY922 (Figure 2).²¹ The present work describes a pure fragment-screening approach that originated from a fragment-like drug molecule containing a phenolamide moiety; the final compounds differ substantially in their architecture and shape from resorcinols such as NYP-AUY922 which contain a five-membered aromatic heterocycle directly attached to the resorcinol ring.^{22,52–56} Kung et al. have described a resorcinol amide series that they identified independently via high throughput screening.^{57,58} The present work differs substantially in the screening and optimization methodology and in the final clinical candidate, which is

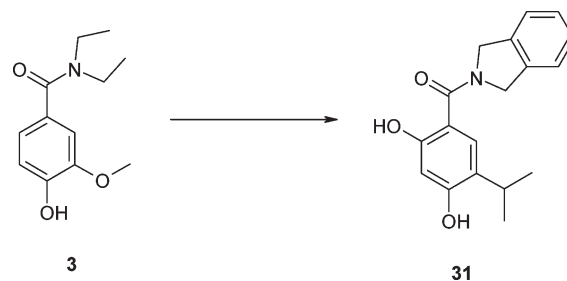


Figure 11. Structure for lead molecule **31** together with fragment **3** from which it was derived. The lead molecule is over 1 000 000 times more potent than the fragment, and this can be decomposed into (i) 110-fold for replacement of the methoxy group by isopropyl as derived from affinities for compound **3** and compound **17** (net increase of one heavy atom), (ii) 100-fold for replacement of the diethylamide with the isoindoline amide as derived from affinities for compound **17** and compound **28** (net increase of four heavy atoms), and (iii) 130-fold for the introduction of the 2-OH group as derived from affinities for compound **28** and compound **31** (net increase of one heavy atom).

described in the companion paper (DOI: 10.1021/jm100060b). Both our series^{59,60} and the series of Kung and co-workers⁶¹ have previously been described in the patent literature.

The literature now contains many Hsp90 medicinal chemistry papers from a large number of groups. Approaches adopted include HTS, fragment screening, virtual screening, and natural product optimization or optimization based on an existing lead.^{16–18} A number of clinical compounds have also been revealed, so it is apparent that all approaches have been successful to some degree and that Hsp90 is a reasonably tractable target from a medicinal chemistry point of view. This paper shows that careful structure-based optimization based on initially very weak fragment hits can deliver highly ligand efficient and low molecular weight leads for Hsp90 without the need for large amounts of synthetic chemistry. In the case of the pyrimidine series, optimization from fragment **1** (250 μ M) to compound **12** (6.3 nM) improved affinity by 40000-fold while the heavy atom count increased by just five atoms. This increase in affinity was mainly gained through the stabilization of the active conformation of the starting fragment and the improvement of hydrophobic contact with the enzyme. Figure 11 and its caption summarize the structure-guided optimization process that led to the resorcinol lead compound **31** (0.54 nM) starting from the phenol fragment **3** (790 μ M). Affinity was improved by over a million-fold with the addition of only six heavy atoms, and this can be ascribed to three changes, each contributing about 100-fold to affinity. The first modification (methoxy to isopropyl) gave superior filling of the proximal lipophilic pocket with a net increase of one heavy atom; the second modification (diethylamide to isoindolamide) was the least “efficient” with a net increase of four heavy atoms and was driven by improved lipophilic contact with the enzyme as a result of the conformational movement of Lys58. The final modification (addition of a hydroxyl group) added one additional heavy atom with the formation of a hydrogen bond with Asp97 and a further water-mediated hydrogen bond. In terms of the efficiency of the added groups,⁶² the two fragment to lead campaigns described in this paper are among the most efficient ever reported. In both cases the final lead has a molecular weight of around 300 Da which leaves a significant amount of “molecular weight head room” to tune the other properties of the molecule during lead optimization. This means that groups

can be added to the molecule to improve nonpotency related properties without the fear that the resulting clinical candidate lies outside druglike space.

In conclusion we have applied a fragment screening approach to Hsp90 and developed two series of compounds starting from fragments. In each series, structure-based drug design led to the discovery of high potency compounds with excellent ligand efficiency. A resorcinol lead with subnanomolar affinity and good cell potency has been identified, and the companion paper (DOI: 10.1021/jm100060b) describes how this lead was converted into a compound that is currently in clinical trials for the treatment of cancer.

Experimental Section

Chemistry. The method employed in determining the purity of compounds was LCMS, and all compounds had purities of >95%. Reagents and solvents were obtained from commercial suppliers and used without further purification. Thin layer chromatography (TLC) analytical separations were conducted with E. Merck silica gel F-254 plates of 0.25 mm thickness and were visualized with UV light (254 nm) and/or stained with iodine, potassium permanganate, or phosphomolybdic acid solutions followed by heating. Flash chromatography was performed either manually using E. Merck silica gel or using an automated Biotage SP4 system with prepacked disposable SiO₂ cartridges (4, 8, 19, 38, 40, and 90 g sizes) with stepped or gradient elution at 5–40 mL/min using the indicated solvent mixture. ¹H nuclear magnetic resonance (NMR) spectra were recorded in the deuterated solvents specified on a Bruker Avance 400 spectrometer operating at 400 MHz. Chemical shifts are reported in parts per million (δ) from the tetramethylsilane resonance in the indicated solvent (TMS: 0.0 ppm). Data are reported as follows: chemical shift, multiplicity (br = broad, s = singlet, d = doublet, t = triplet, m = multiplet), integration. Compound purity and mass spectra were determined by a Waters 2795/Platform LC LC/MS system using the positive electrospray ionization technique (+ESI), a Waters Fractionlynx/Micromass ZQ LC/MS system using the positive electrospray ionization technique (+ESI), or an Agilent 1200SL-6140 LC/MS system using positive-negative switching, using a mobile phase of acetonitrile/water with 0.1% formic acid.

4-(3-Pyridyl)pyrimidin-2-ylamine **1**, 2-aminopyrimidine **2**, 4, *N,N*-diethyl-3-methoxy-4-hydroxybenzamide **3**, 2-chloro-4-methylphthalazine **4**, 4-chloro-(6-phenyl)pyrimidin-2-ylamine **5**, 3-chloro-4-hydroxybenzoic acid, 3-*tert*-butyl-4-hydroxybenzoic acid, and 5-*tert*-butyl-2-methoxybenzoic acid are commercially available. 5-Isopropyl-2-methoxybenzoic acid,⁶³ 3-ethyl-4-hydroxybenzoic acid,⁶⁴ and 2,4-bis-benzyloxy-5-isopropenylbenzoic acid⁵⁹ were prepared as described previously. 4-Hydroxy-3-isopropylbenzoic acid was prepared from 2-isopropylphenol according to the method described⁶⁴ for the synthesis of 3-ethyl-4-hydroxybenzoic acid. Experimental and spectroscopic details for all other noncommercially available compounds are given below or are available in the Supporting Information.

4-Chloro-6-[2,4-dichloro-5-(2-morpholin-4-ylethoxy)phenyl]pyrimidin-2-ylamine (14). Concentrated HCl (19 mL) was added to 5-(benzyloxy)-2,4-dichloroaniline (52 g, 19.3 mmol, 1.0 equiv) in glacial acetic acid (77 mL), and the mixture was cooled in an ice–water bath. Sodium nitrite (1.5 g, 22.2 mmol, 1.2 equiv) was added in water (64 mL) slowly, maintaining the temperature at <5 °C. This was stirred for 30 min. This mixture was poured into KI (6.4 g, 38.6 mmol, 2.0 equiv) and I₂ (1.7 g, 5.4 mmol, 0.3 equiv) in water (241 mL) and was left to stir for 1.5 h at room temperature. The reaction was quenched by diluting with water and extracting the product with dichloromethane ($\times 3$). The combined organic layers were washed with brine and dried over MgSO₄. The product was filtered and concentrated to dryness under reduced pressure to leave

1-benzyloxy-2,4-dichloro-5-iodobenzene as a brown oil. The product was taken on without further purification. To 1-benzyloxy-2,4-dichloro-5-iodobenzene (4.5 g, 11.9 mmol, 1.0 equiv) in tetrahydrofuran (40 mL) at –78 °C was added the triisopropyl borate (3.4 g, 17.8 mmol, 1.5 equiv) and then the *n*-BuLi (11.1 mL, 1.6 M, 1.5 equiv) slowly. The mixture was allowed to stir for an hour, and the reaction was then quenched with NH₄Cl (sat., aq.). The mixture was allowed to warm to room temperature and was diluted with water and ethyl acetate. The product was extracted with ethyl acetate ($\times 3$). The combined organic layers were washed with brine and dried over MgSO₄. The product was filtered and concentrated to dryness under reduced pressure to leave a pale-yellow oil. The crude reaction mixture was coupled to 2-amino-4,6-dichloropyrimidine following the same procedure as for pyrimidine **7**, except the reaction was heated thermally at 50 °C for 3 h. The title compound was isolated by preparative HPLC to yield the product as a colorless solid. ¹H NMR (400 MHz, Me-*d*₃-OD) δ 7.60 (s, 1H), 7.49 (d, 2H), 7.45–7.32 (m, 4H), 6.93 (s, 1H), 5.22 (s, 2H). LCMS (ESI): *m/z* 380 (M + H⁺).

To 4-(5-benzyloxy-2,4-dichlorophenyl)-6-chloropyrimidin-2-ylamine (5.0 g, 9.2 mmol, 1.0 equiv) in dichloromethane (31 mL) was added BCl₃ (10.1 mL, 10.1 mmol, 1.1 equiv) at –78 °C under a nitrogen atmosphere. The mixture was stirred for 2 h. The reaction was then quenched with methanol (10 mL), and the mixture was allowed to warm to room temperature. The mixture was then diluted with water, and the product was extracted with ethyl acetate ($\times 3$). The combined organic layers were washed with water, brine and dried over MgSO₄. The product was filtered and concentrated to dryness under reduced pressure to leave a pale-yellow oil. The product was purified by column chromatography (*R_f* = 0.48, 100% diethyl ether) to yield 5-(2-amino-6-chloropyrimidin-4-yl)-2,4-dichlorophenol as a colorless solid. ¹H NMR (400 MHz, Me-*d*₃-OD) δ 7.48 (s, 1H), 7.11 (s, 1H), 6.90 (s, 1H). LCMS (ESI): *m/z* 290 (M + H⁺).

To 5-(2-amino-6-chloropyrimidin-4-yl)-2,4-dichlorophenol (81 mg, 0.28 mmol, 1.0 equiv) in DMF (3 mL) was added Cs₂CO₃ (199 mg, 0.61 mmol, 2.1 equiv) and then *N*-(2-chloroethyl)morpholine·HCl (57 mg, 0.31 mmol, 1.1 equiv) under a nitrogen atmosphere. The mixture was heated thermally at 80 °C for 3 h. The mixture was allowed to cool and concentrated to dryness under reduced pressure. The title compound **14** was crystallized from methanol to yield the product as beige crystals. ¹H NMR (400 MHz, Me-*d*₃-OD) δ 7.58 (s, 1H), 7.33 (s, 1H), 6.96 (s, 1H), 4.27 (t, 2H), 3.72 (dd, 4H), 2.88 (t, 2H), 2.66 (dd, 4H). LCMS (ESI): *m/z* 403 (M + H⁺). LCMS purity: 96.7%.

4-(2,4-Dihydroxy-5-isopropylbenzoyl)morpholine (30). Morpholine (66 mg, 0.75 mmol) was added to a stirred mixture of 2,4-bis-benzyloxy-5-isopropenylbenzoic acid (187 mg, 0.5 mmol), 1-(3-dimethylaminopropyl)-3-ethylcarbodiimide hydrochloride (116 mg, 1.2 mmol), and 1-hydroxybenzotriazole (81 mg, 0.6 mmol) in dichloromethane (10 mL), and the mixture was stirred at room temperature for 4 h. The mixture was washed successively with 2 M hydrochloric acid, saturated sodium bicarbonate, and water. The organic layer was separated and concentrated under reduced pressure to afford 4-(2,4-bis-benzyloxy-5-isopropenylbenzoyl)morpholine as a colorless solid. Yield: 76%. ¹H NMR (DMSO-*d*₆) δ 7.57–7.30 (m, 10H), 7.02 (s, 1H), 6.95 (s, 1H), 5.18 (d, 4H), 5.06 (d, 2H), 3.57 (br s, 4H), 3.41 (br s, 2H), 3.16 (br s, 2H), 2.03 (s, 3H). LCMS (+ESI): *m/z* 444 (M + H⁺). LCMS purity: 95.8%.

4-(2,4-Bis-benzyloxy-5-isopropenylbenzoyl)morpholine (133 mg, 0.3 mmol) was dissolved in methanol (8 mL), 10% palladium on carbon (50 mg) was added, and the mixture was stirred overnight under a hydrogen atmosphere at room temperature. The mixture was filtered, the solids were rinsed with methanol (4 mL), and the combined filtrates were reduced to dryness under reduced pressure to afford **30** as a colorless solid. Yield: 90%. ¹H NMR (DMSO-*d*₆): δ 9.57 (br s, 1H), 6.85 (s, 1H), 6.36 (s, 1H), 3.56 (br m, 4H), 3.40 (br s, 4H), 3.06 (m, 1H), 1.10 (d, 6H). LCMS (+ESI): *m/z* 266 (M + H⁺). LCMS purity: 97.1%.

2-(2,4-Dihydroxy-5-isopropylbenzoyl)-2,3-dihydro-1H-isoindole (31). Compound **31** was prepared in a similar manner to **30** from 2,3-dihydro-1H-isoindole and 2,4-bis-benzyloxy-5-isopropenylbenzoic acid. ^1H NMR (DMSO- d_6): δ 10.04 (s, 1H), 9.64 (s, 1H), 7.31 (br m, 4H, s), 7.04 (s, 1H), 6.41 (s, 1H), 4.77 (s, 4H), 3.10 (m, 1H), 1.14 (d, 6H, d). LCMS (+ESI): m/z 298 (M + H $^+$). LCMS purity: 100.0%.

NMR Screening. NMR experiments were carried out at 500 MHz, using a Bruker DRX500 instrument equipped with a TXI cryoprobe. The N-terminal domain of Hsp90 was expressed and purified as described below, giving a product of molecular mass 24 508 Da, whose mass was confirmed by time-of-flight mass spectrometry. Samples for NMR screening were prepared in 20 mM Tris buffer, pH 7.4, containing 200 μM ADP, 150 mM NaCl, 1 mM BME, and 10% D $_2$ O. Typical screening samples contained 0.3 mg/mL (12.5 μM) Hsp90 and four fragments, each at 500 μM (2% DMSO). This gave a molar ratio of fragment to target of 40:1, a typical value for water-LOGSY experiments.⁴⁴ At these protein and ligand concentrations, fragments that bind with dissociation constants better than 1 mM are expected to be detected. LOGSY experiments were performed using the e-PHOGSY sequence of Dalvit et al. incorporating a 1 s delay to allow cross-relaxation between fragments and water, and a 100 ms CPMG period during which time any protein magnetization decays.⁶⁵

In order to enhance the LOGSY signal, all NMR experiments were performed at 5 °C. Lowering the temperature improves the affinities of ligands that bind exothermically and reduces the rates of exchange between bulk water and water of hydration, leading to improved LOGSY intensities. In order to detect the small positive LOGSY effects caused by binding to the protein target, LOGSY spectra were obtained in the presence and the absence of the protein target, and these spectra were directly compared.

The LOGSY spectra were defined as medium or strong signals as follows. LOGSY spectra were obtained from two separate samples (+protein and buffer control), and these were subtracted (+protein – buffer control) to give the LOGSY difference spectrum. This spectrum shows the change in the amount of magnetization transferred from water to the ligands, due to protein binding. The intensity of each peak in this spectrum depends on a number of experimental choices (number of scans, magnetization transfer time, relaxation delays, etc.), and there is no reference spectrum generated with which to quantitate the LOGSY effects. However a standard 1D spectrum was also run (with fewer scans and different relaxation delays) and the LOGSY intensity was compared with this. For each compound, the largest % LOGSY signal observed for any detectable aromatic proton was recorded. The % LOGSY values for ligands against HSP90 (LOGSY intensity versus 1D intensity) ranged from 0 to about 60% with strong LOGSY signals being defined as > 20% and medium signals defined as 11–20%.

The presence of 200 μM ADP in the buffer enabled fragment hits, which had been identified by changes in their LOGSY signals, to be further characterized according to their competition at the nucleotide site, determined by a reduction in the LOGSY signal of ADP. In the absence of Mg $^{2+}$, 200 μM corresponds to a concentration of ADP around its dissociation constant so that the presence of ADP does not greatly reduce the sensitivity of the experiment to fragment binding while providing a convenient method of identifying cocktails that contain an active-site ligand. LOGSY spectra were reacquired after the addition of a small aliquot of a concentrated MgCl $_2$ solution to the screening solutions, giving a final concentration of 5 mM. This converts ADP to its Mg $^{2+}$ complex which binds more tightly to Hsp90, with a dissociation constant measured by ITC of approximately 10 μM . This in turn leads to complete displacement of fragments that bind exclusively to the active site of Hsp90, enabling selective active-site binders to be readily identified.

Crystallography. Two hexahistidine tagged N-terminal fragments (9-236 and 9-224) of Hsp90 α were cloned into a pET28 vector and expressed in BL21 (DE3). The proteins were captured using a Ni $^{2+}$ affinity column followed by removal of the tag using thrombin and final purification on a Superdex 75 gel filtration column with a final buffer of 20 mM Tris-HCl (pH 7.4), 150 mM NaCl, and 1 mM β -ME. The proteins were concentrated to between 20 and 25 mg mL $^{-1}$ prior to crystallization. For soaking experiments, two crystal forms were exploited because of the differing loop structure around the active site. The I222 apo crystals were generated using the hanging drop, vapor diffusion method by combining equal volumes of protein and mother liquor (0.1 M Hepes-NaOH, pH 7.2, 0.2 M magnesium chloride, 20% (w/v) MPEG 2000). Structures for compounds **2**, **4**, **2 + 4**, and **14** were obtained in this system. The P2 $_1$ back-soakable crystals were also generated using the hanging drop, vapor diffusion method but 2 mM ADP·Mg $^{2+}$ was added to the protein before combining with mother liquor (0.1 M Bis-Tris, pH 6.0, 0.2 M ammonium phosphate, 25% (w/v) PEG 3350). Structures for compounds **6**, **18**, and **21** were obtained in this system. All crystallization experiments were performed at 4 °C and usable crystals appeared between 1 and 3 days. Soaking was performed in respective mother liquors containing 20% glycerol and 50 mM compound with a final DMSO concentration of 10% (v/v) for periods of up to 24 h. Crystals were subsequently flash frozen and data collected on a Rigaku RU-H3R rotating anode generator with Osmic confocal blue optics and either a Jupiter CCD or Raxis 4++ image plate. For cocrystallization, the protein was mixed with 5 mM compound with a final DMSO concentration of 2.5% (v/v), followed by automated crystallization setup using a Cartesian robot, typically at 0.2 μL final drop volumes in sitting drop 96-well formats using a limited in house designed matrix of crystallization conditions. Crystals grown using this system were extracted from the low volume drops, cryoprotected in mother liquor with 20% glycerol, and flash frozen for in house data collection. Compound **1** crystals were grown in 0.1 M Bis-Tris, pH 5.5, 0.2 M ammonium acetate, 25% PEG 3350. Compound **3** crystals were grown in 0.1 M Bis-Tris, pH 5.75, 0.2 M ammonium acetate, 20% PEG 3350. Compound **24** crystals were grown in 0.1 M Bis-Tris, pH 5.25, 0.2 M ammonium acetate, 27% PEG 3350. Compound **31** crystals were grown in 0.1 M Tris-HCl, pH 8.0, 0.2 M magnesium chloride, 22% PEG 4000.

Diffraction data were processed using MOSFLM⁶⁶ and CCP4.⁶⁷ The structures were solved using isomorphous replacement with the coordinates previously described, 1YER⁶⁸ for the I222 form and 1BYQ⁶⁹ for the P2 $_1$ back-soakable and cocrystallization form. The structures were refined using REFMAC⁷⁰ and Buster-TNT.⁷¹ Ligands were placed using AutoSolve⁷² and manual rebuilds made in AstexViewer⁷³ and COOT.⁷⁴ Final validation checks were performed using Procheck,⁷⁵ prior to deposition of coordinates and structure factors into the PDB.

Isothermal Titration Calorimetry (ITC). ITC experiments were performed on a MicroCal VP-ITC at 25 °C in a buffer comprising 25 mM Tris, 100 mM NaCl, 1 mM MgCl $_2$, and 1 mM TCEP at pH 7.4. The final DMSO concentration was between 1% and 5%. The protein used was the same Hsp90 N-terminal ATPase domain construct used in both the NMR and X-ray crystallography work. Most of ITC experiments were set up with protein in the sample cell and compound in the injection syringe, although in cases where compound solubility was limiting, this was reversed. Data were fit to a single site binding model using Origin 7.0 software. All the stoichiometry values from the data analysis were in the range 0.8–1.3, providing an excellent internal control for the quality, purity, and stability of both the protein and the compounds. Replicate experiments indicate that errors in the dissociation constants are generally better than 2-fold. The stoichiometry parameter was fixed at 1 in cases where the K $_d$ value was greater than the protein

concentration.⁷⁶ By use of the procedure outlined above, ADP and 17-DMAG had measured dissociation constants of 9.2 and 0.21 μM . These values are in good agreement with literature dissociation constants with the full length human Hsp90 protein of 11 μM for ADP and 0.35 μM for 17-DMAG.⁷⁷ These results indicate that ITC on N-terminal Hsp90 is a good surrogate for ITC on full length Hsp90, provided the compounds bind in the ATPase active site. A competition format ITC⁷⁸ was necessary to accurately determine the affinity of compound **31**. This required preincubating the protein with one of our moderately potent phenol compounds in the sample cell prior to initiating the titration with compound **31**. A competition binding model was used to fit the data and obtain a K_d estimate for compound **31**. More experimental detail on ITC is given in Supporting Information together with representative data for three compounds of different affinity (i.e., compounds **1**, **5**, and **31**).

Calculation of the Torsion Energy Profile. All energies were calculated using the ab initio quantum chemistry package Q-Chem.⁷⁹ To calculate the torsion energy profile, a torsion scan was carried out on a Corina generated structure by varying the desired torsion angle between 0° and 180°, in 15° intervals. For each structure at a given torsion angle, a constrained energy minimization (basis set, 3-21G*; method, Hartree-Fock) was carried out with a single constraint on the torsion angle to restrain the molecule to the specific torsion angle value while the rest of the molecule was geometrically optimized. The energy of the optimized molecule at the specified conformational torsion was then calculated using B3LYP method with 6-311G* basis set. Finally, the 12 energies were utilized to estimate approximately the relative population of each conformation using a Boltzman distribution.

Virtual Screening. The X-ray crystal structure of the N-terminal domain of Hsp90 complexed with compound **1** was used to virtual-screen aminopyrimidine analogues of **1**. Water molecules were removed from the structure with the exception of the four conserved waters at the bottom of the ATP binding pocket. Hydrogens were added to the protein and waters, and a binding pocket was generated with all protein and water atoms within 6 Å of any non-hydrogen atom in ligand **1**. This binding site was used to run all dockings and virtual screens in the presence of the key water molecules, allowing them to toggle on/off and spin around their three principal axes with methods and settings previously described by Verdonk et al.⁸⁰ All calculations were run on a Linux cluster using the Astex Web-based virtual screening platform.⁸¹ A number of filters (heavy atom count, molecular weight, number of donors, number of acceptors, ClogP, and polar surface area) combined with the scoring functions Goldscore⁸² and Chemscore^{83,84} were applied to score and to rank the docked libraries. Of the two scoring functions, Goldscore performed generally better in terms of reproducing the correct binding modes observed in Hsp90 X-ray crystal structures. Finally, virtual screens were visually analyzed, and molecules were selected on the basis of the binding mode, the chemical tractability, and the calculated score.

Hsp90 Cell Assay and Western Blot. The antiproliferative activities of the compounds were determined by measuring their ability to inhibit the growth of HCT116 cells (obtained from European Collection of Cell Cultures). Cell growth was measured using the Alamar blue assay as described in Squires et al.⁸⁵

For Western blotting experiments, HCT116 cells were treated with compound in six-well tissue culture plates at the stated concentrations for 18 h before washing with PBS and lysing cells by the addition of ice-cold lysis buffer (40 mM Tris-HCl (pH 7.5), 274 mM NaCl, 20% glycerol, 2% Triton-X-100, 1 mM Na_3VO_4 , 50 mM NaF, 1% protease inhibitor cocktail set III (Calbiochem)). The cells were lysed on ice for 30 min and clarified by centrifugation. Lysates in SDS sample buffer were heated for 5 min at 95 °C, resolved by SDS-PAGE, and immunoblotted with the indicated antibodies followed by either infrared dye labeled anti-rabbit or anti-mouse antibodies

(LICOR). Antibodies were sourced as follows: CDK4 from Santa Cruz Antibodies (Santa Cruz CA), Hsp70 from StressGen Biotechnologies (Victoria, British Columbia, Canada), and GAPDH from Chemicon International (Temecula, CA). Blots were scanned to detect infrared fluorescence on the Odyssey infrared imaging system (LICOR).

Acknowledgment. The authors thank Anne Cleasby, David Rees, Brian Williams, Lyn Leaper, Harren Jhoti, Robin Carr, Neil Thompson, and John Lyons for comments on the manuscript and for providing support to the project.

Supporting Information Available: Additional synthetic chemistry experimental information, additional ITC experimental information, and representative examples of ITC data. This material is available free of charge via the Internet at <http://pubs.acs.org>.

References

- (1) Bukau, B.; Weissman, J.; Horwich, A. Molecular chaperones and protein quality control. *Cell* **2006**, *125*, 443–451.
- (2) Workman, P.; Burrows, F.; Neckers, L.; Rosen, N. Drugging the cancer chaperone HSP90: combinatorial therapeutic exploitation of oncogene addiction and tumor stress. *Ann. N.Y. Acad. Sci.* **2007**, *1113*, 202–216.
- (3) Whitesell, L.; Lindquist, S. L. HSP90 and the chaperoning of cancer. *Nat. Rev. Cancer* **2005**, *5*, 761–772.
- (4) Hanahan, D.; Weinberg, R. A. The hallmarks of cancer. *Cell* **2000**, *100*, 57–70.
- (5) Workman, P. Combinatorial attack on multistep oncogenesis by inhibiting the Hsp90 molecular chaperone. *Cancer Lett.* **2004**, *206*, 149–157.
- (6) Chiosis, G.; Neckers, L. Tumor selectivity of Hsp90 inhibitors: the explanation remains elusive. *ACS Chem. Biol.* **2006**, *1*, 279–284.
- (7) Kamal, A.; Thao, L.; Sensintaffar, J.; Zhang, L.; Boehm, M. F.; Fritz, L. C.; Burrows, F. J. A high-affinity conformation of Hsp90 confers tumour selectivity on Hsp90 inhibitors. *Nature* **2003**, *425*, 407–410.
- (8) Solit, D. B.; Chiosis, G. Development and application of Hsp90 inhibitors. *Drug Discovery Today* **2008**, *13*, 38–43.
- (9) Pearl, L. H.; Prodromou, C. Structure and mechanism of the Hsp90 molecular chaperone machinery. *Annu. Rev. Biochem.* **2006**, *75*, 271–294.
- (10) Vilenchik, M.; Solit, D.; Basso, A.; Huezio, H.; Lucas, B.; He, H.; Rosen, N.; Spampinato, C.; Modrich, P.; Chiosis, G. Targeting wide-range oncogenic transformation via PU24FC1, a specific inhibitor of tumor Hsp90. *Chem. Biol.* **2004**, *11*, 787–797.
- (11) Soga, S.; Shiotsu, Y.; Akinaga, S.; Sharma, S. V. Development of radicicol analogues. *Curr. Cancer Drug Targets* **2003**, *3*, 359–369.
- (12) Neckers, L.; Schulte, T. W.; Mimnaugh, E. Geldanamycin as a potential anti-cancer agent: its molecular target and biochemical activity. *Invest. New Drugs* **1999**, *17*, 361–373.
- (13) Ge, J.; Normant, E.; Porter, J. R.; Ali, J. A.; Dembski, M. S.; Gao, Y.; Georges, A. T.; Grenier, L.; Pak, R. H.; Patterson, J.; Sydor, J. R.; Tibbitts, T. T.; Tong, J. K.; Adams, J.; Palombella, V. J. Design, synthesis, and biological evaluation of hydroquinone derivatives of 17-amino-17-demethoxygeldanamycin as potent, water-soluble inhibitors of Hsp90. *J. Med. Chem.* **2006**, *49*, 4606–4615.
- (14) Kaur, G.; Belotti, D.; Burger, A. M.; Fisher-Nielson, K.; Borsotti, P.; Riccardi, E.; Thillainathan, J.; Hollingshead, M.; Sausville, E. A.; Giavazzi, R. Antiangiogenic properties of 17-(dimethylaminoethylamino)-17-demethoxygeldanamycin: an orally bioavailable heat shock protein 90 modulator. *Clin. Cancer Res.* **2004**, *10*, 4813–4821.
- (15) Schulte, T. W.; Neckers, L. M. The benzoquinone ansamycin 17-allylamino-17-demethoxygeldanamycin binds to HSP90 and shares important biologic activities with geldanamycin. *Cancer Chemother. Pharmacol.* **1998**, *42*, 273–279.
- (16) Drysdale, M. J.; Brough, P. A. Medicinal chemistry of Hsp90 inhibitors. *Curr. Top. Med. Chem.* **2008**, *8*, 859–868.
- (17) Janin, Y. L. Heat shock protein 90 inhibitors. A text book example of medicinal chemistry? *J. Med. Chem.* **2005**, *48*, 7503–7512.
- (18) Blegg, B. S.; Kerr, T. D. Hsp90 inhibitors: small molecules that transform the Hsp90 protein folding machinery into a catalyst for protein degradation. *Med. Res. Rev.* **2006**, *26*, 310–338.

- (19) Sgobba, M.; Rastelli, G. Structure-based and in silico design of Hsp90 inhibitors. *ChemMedChem* **2009**, *4*, 1399–1409.
- (20) Brough, P. A.; Barril, X.; Borgognoni, J.; Chene, P.; Davies, N. G.; Davis, B.; Drysdale, M. J.; Dymock, B.; Eccles, S. A.; Garcia-Echeverria, C.; Fromont, C.; Hayes, A.; Hubbard, R. E.; Jordan, A. M.; Jensen, M. R.; Massey, A.; Merrett, A.; Padfield, A.; Parsons, R.; Radimerski, T.; Raynaud, F. I.; Robertson, A.; Roughley, S. D.; Schoepfer, J.; Simmonite, H.; Sharp, S. Y.; Surgenor, A.; Valenti, M.; Walls, S.; Webb, P.; Wood, M.; Workman, P.; Wright, L. Combining hit identification strategies: fragment-based and in silico approaches to orally active 2-aminothieno[2,3-*d*]pyrimidine inhibitors of the Hsp90 molecular chaperone. *J. Med. Chem.* **2009**, *52*, 4794–4809.
- (21) Eccles, S. A.; Massey, A.; Raynaud, F. I.; Sharp, S. Y.; Box, G.; Valenti, M.; Patterson, L.; de Haven, B. A.; Gowan, S.; Boxall, F.; Aherne, W.; Rowlands, M.; Hayes, A.; Martins, V.; Urban, F.; Boxall, K.; Prodromou, C.; Pearl, L.; James, K.; Matthews, T. P.; Cheung, K. M.; Kalusa, A.; Jones, K.; McDonald, E.; Barril, X.; Brough, P. A.; Cansfield, J. E.; Dymock, B.; Drysdale, M. J.; Finch, H.; Howes, R.; Hubbard, R. E.; Surgenor, A.; Webb, P.; Wood, M.; Wright, L.; Workman, P. NVP-AUY922: a novel heat shock protein 90 inhibitor active against xenograft tumor growth, angiogenesis, and metastasis. *Cancer Res.* **2008**, *68*, 2850–2860.
- (22) Brough, P. A.; Aherne, W.; Barril, X.; Borgognoni, J.; Boxall, K.; Cansfield, J. E.; Cheung, K. M.; Collins, I.; Davies, N. G.; Drysdale, M. J.; Dymock, B.; Eccles, S. A.; Finch, H.; Fink, A.; Hayes, A.; Howes, R.; Hubbard, R. E.; James, K.; Jordan, A. M.; Lockie, A.; Martins, V.; Massey, A.; Matthews, T. P.; McDonald, E.; Northfield, C. J.; Pearl, L. H.; Prodromou, C.; Ray, S.; Raynaud, F. I.; Roughley, S. D.; Sharp, S. Y.; Surgenor, A.; Walmsley, D. L.; Webb, P.; Wood, M.; Workman, P.; Wright, L. 4,5-Diarylisoazole Hsp90 chaperone inhibitors: potential therapeutic agents for the treatment of cancer. *J. Med. Chem.* **2008**, *51*, 196–218.
- (23) Bao, R.; Lai, C. J.; Qu, H.; Wang, D.; Yin, L.; Zifcak, B.; Atoyan, R.; Wang, J.; Samson, M.; Forrester, J.; Della Rocca, S.; Xu, G. X.; Tao, X.; Zhai, H. X.; Cai, X.; Qian, C. CUDC-305, a novel synthetic HSP90 inhibitor with unique pharmacologic properties for cancer therapy. *Clin. Cancer Res.* **2009**, *15*, 4046–4057.
- (24) Huang, K. H.; Veal, J. M.; Fadden, R. P.; Rice, J. W.; Eaves, J.; Strachan, J. P.; Barabasz, A. F.; Foley, B. E.; Barta, T. E.; Ma, W.; Silinski, M. A.; Hu, M.; Partridge, J. M.; Scott, A.; DuBois, L. G.; Freed, T.; Steed, P. M.; Ommen, A. J.; Smith, E. D.; Hughes, P. F.; Woodward, A. R.; Hanson, G. J.; McCall, W. S.; Markworth, C. J.; Hinkley, L.; Jenks, M.; Geng, L.; Lewis, M.; Otto, J.; Pronk, B.; Verleysen, K.; Hall, S. E. Discovery of novel 2-aminobenzamide inhibitors of heat shock protein 90 as potent, selective and orally active antitumor agents. *J. Med. Chem.* **2009**, *52*, 4288–4305.
- (25) Lundgren, K.; Zhang, H.; Brekken, J.; Huser, N.; Powell, R. E.; Timple, N.; Busch, D. J.; Neely, L.; Sensintaffar, J. L.; Yang, Y. C.; McKenzie, A.; Friedman, J.; Scannevin, R.; Kamal, A.; Hong, K.; Kasibhatla, S. R.; Boehm, M. F.; Burrows, F. J. BIIB021, an orally available, fully synthetic small-molecule inhibitor of the heat shock protein Hsp90. *Mol. Cancer Ther.* **2009**, *8*, 921–929.
- (26) Erlanson, D. A.; McDowell, R. S.; O'Brien, T. Fragment-based drug discovery. *J. Med. Chem.* **2004**, *47*, 3463–3482.
- (27) Rees, D. C.; Congreve, M.; Murray, C. W.; Carr, R. Fragment-based lead discovery. *Nat. Rev. Drug Discovery* **2004**, *3*, 660–672.
- (28) Erlanson, D. A. Fragment-based lead discovery: a chemical update. *Curr. Opin. Biotechnol.* **2006**, *17*, 643–652.
- (29) Fattori, D. Molecular recognition: the fragment approach in lead generation. *Drug Discovery Today* **2004**, *9*, 229–238.
- (30) Hajduk, P. J.; Greer, J. A decade of fragment-based drug design: strategic advances and lessons learned. *Nat. Rev. Drug Discovery* **2007**, *6*, 211–219.
- (31) Alex, A. A.; Flocco, M. M. Fragment-based drug discovery: what has it achieved so far? *Curr. Top. Med. Chem.* **2007**, *7*, 1544–1567.
- (32) Congreve, M.; Chessari, G.; Tisi, D.; Woodhead, A. J. Recent developments in fragment-based drug discovery. *J. Med. Chem.* **2008**, *51*, 3661–3680.
- (33) Chessari, G.; Woodhead, A. J. From fragment to clinical candidate—a historical perspective. *Drug Discovery Today* **2009**, *14*, 668–675.
- (34) Schulz, M. N.; Hubbard, R. E. Recent progress in fragment-based lead discovery. *Curr. Opin. Pharmacol.* **2009**, *9*, 615–621.
- (35) Leeson, P. D.; Springthorpe, B. The influence of drug-like concepts on decision-making in medicinal chemistry. *Nat. Rev. Drug Discovery* **2007**, *6*, 881–890.
- (36) Lipinski, C. A.; Lombardo, F.; Dominy, B. W.; Feeney, P. J. Experimental and computational approaches to estimate solubility and permeability in drug discovery and development settings. *Adv. Drug Delivery Rev.* **2001**, *46*, 3–26.
- (37) Vieth, M.; Siegel, M. G.; Higgs, R. E.; Watson, I. A.; Robertson, D. H.; Savin, K. A.; Durst, G. L.; Hipskind, P. A. Characteristic physical properties and structural fragments of marketed oral drugs. *J. Med. Chem.* **2004**, *47*, 224–232.
- (38) Wenlock, M. C.; Austin, R. P.; Barton, P.; Davis, A. M.; Leeson, P. D. A comparison of physicochemical property profiles of development and marketed oral drugs. *J. Med. Chem.* **2003**, *46*, 1250–1256.
- (39) Hopkins, A. L.; Groom, C. R.; Alex, A. Ligand efficiency: a useful metric for lead selection. *Drug Discovery Today* **2004**, *9*, 430–431.
- (40) Kuntz, I. D.; Chen, K.; Sharp, K. A.; Kollman, P. A. The maximal affinity of ligands. *Proc. Natl. Acad. Sci. U.S.A.* **1999**, *96*, 9997–10002.
- (41) Leach, A. R.; Hann, M. M.; Burrows, J. N.; Griffen, E. J. Fragment screening: an introduction. *Mol. BioSyst.* **2006**, *2*, 430–446.
- (42) Hann, M. M.; Leach, A. R.; Harper, G. Molecular complexity and its impact on the probability of finding leads for drug discovery. *J. Chem. Inf. Comput. Sci.* **2001**, *41*, 856–864.
- (43) Hartshorn, M. J.; Murray, C. W.; Cleasby, A.; Frederickson, M.; Tickle, I. J.; Jhoti, H. Fragment-based lead discovery using X-ray crystallography. *J. Med. Chem.* **2005**, *48*, 403–413.
- (44) Dalvit, C.; Fogliatto, G.; Stewart, A.; Veronesi, M.; Stockman, B. WaterLOGSY as a method for primary NMR screening: practical aspects and range of applicability. *J. Biomol. NMR* **2001**, *21*, 349–359.
- (45) Wolfson, B.; Siker, E. S.; Ciccarelli, H. E. A double blind comparison of doxapram, ethamivan and methylphenidate. *Am. J. Med. Sci.* **1965**, *249*, 391–398.
- (46) Roe, S. M.; Prodromou, C.; O'Brien, R.; Ladbury, J. E.; Piper, P. W.; Pearl, L. H. Structural basis for inhibition of the Hsp90 molecular chaperone by the antitumor antibiotics radicicol and geldanamycin. *J. Med. Chem.* **1999**, *42*, 260–266.
- (47) Wright, L.; Barril, X.; Dymock, B.; Sheridan, L.; Surgenor, A.; Beswick, M.; Drysdale, M.; Collier, A.; Massey, A.; Davies, N.; Fink, A.; Fromont, C.; Aherne, W.; Boxall, K.; Sharp, S.; Workman, P.; Hubbard, R. E. Structure–activity relationships in purine-based inhibitor binding to HSP90 isoforms. *Chem. Biol.* **2004**, *11*, 775–785.
- (48) Huth, J. R.; Park, C.; Petros, A. M.; Kunzer, A. R.; Wendt, M. D.; Wang, X.; Lynch, C. L.; Mack, J. C.; Swift, K. M.; Judge, R. A.; Chen, J.; Richardson, P. L.; Jin, S.; Tahir, S. K.; Matayoshi, E. D.; Dorwin, S. A.; Lador, U. S.; Severin, J. M.; Walter, K. A.; Bartley, D. M.; Fesik, S. W.; Elmore, S. W.; Hajduk, P. J. Discovery and design of novel HSP90 inhibitors using multiple fragment-based design strategies. *Chem. Biol. Drug Des.* **2007**, *70*, 1–12.
- (49) Barker, J. J.; Barker, O.; Boggio, R.; Chauhan, V.; Cheng, R. K.; Corden, V.; Courtney, S. M.; Edwards, N.; Falque, V. M.; Fusar, F.; Gardiner, M.; Hamelin, E. M.; Hestekamp, T.; Ichihara, O.; Jones, R. S.; Mather, O.; Mercurio, C.; Minucci, S.; Montalbetti, C. A.; Muller, A.; Patel, D.; Phillips, B. G.; Varasi, M.; Whittaker, M.; Winkler, D.; Yarnold, C. J. Fragment-based identification of Hsp90 inhibitors. *ChemMedChem* **2009**, *4*, 963–966.
- (50) Allen, F. H. The Cambridge Structural Database: a quarter of a million crystal structures and rising. *Acta Crystallogr. B* **2002**, *58*, 380–388.
- (51) Chessari, G.; Congreve, M.; Callaghan, O.; Cowan, S.; Murray, C. W.; Woolford, A. J.; O'Brien, M. A.; Woodhead, A. J. Preparation of Azinamines as Modulators of Heat Shock Protein 90 (Hsp90). WO2006123165, 2006.
- (52) Feldman, R. I.; Mintzer, B.; Zhu, D.; Wu, J. M.; Biroc, S. L.; Yuan, S.; Emayan, K.; Chang, Z.; Chen, D.; Arnaiz, D. O.; Bryant, J.; Ge, X. S.; Whitlow, M.; Adler, M.; Polokoff, M. A.; Li, W. W.; Ferrer, M.; Sato, T.; Gu, J. M.; Shen, J.; Tseng, J. L.; Dinter, H.; Buckman, B. Potent triazolothione inhibitor of heat-shock protein-90. *Chem. Biol. Drug Des.* **2009**, *74*, 43–50.
- (53) Cikotiene, I.; Kazlauskas, E.; Matuliene, J.; Michailoviene, V.; Torresan, J.; Jachno, J.; Matulis, D. 5-Aryl-4-(5-substituted-2,4-dihydroxyphenyl)-1,2,3-thiadiazoles as inhibitors of Hsp90 chaperone. *Bioorg. Med. Chem. Lett.* **2009**, *19*, 1089–1092.
- (54) Cheung, K. M.; Matthews, T. P.; James, K.; Rowlands, M. G.; Boxall, K. J.; Sharp, S. Y.; Maloney, A.; Roe, S. M.; Prodromou, C.; Pearl, L. H.; Aherne, G. W.; McDonald, E.; Workman, P. The identification, synthesis, protein crystal structure and in vitro biochemical evaluation of a new 3,4-diarylpyrazole class of Hsp90 inhibitors. *Bioorg. Med. Chem. Lett.* **2005**, *15*, 3338–3343.
- (55) Dymock, B. W.; Barril, X.; Brough, P. A.; Cansfield, J. E.; Massey, A.; McDonald, E.; Hubbard, R. E.; Surgenor, A.; Roughley, S. D.; Webb, P.; Workman, P.; Wright, L.; Drysdale, M. J. Novel, potent small-molecule inhibitors of the molecular chaperone Hsp90 discovered through structure-based design. *J. Med. Chem.* **2005**, *48*, 4212–4215.

- (56) Gopalsamy, A.; Shi, M.; Golas, J.; Vogan, E.; Jacob, J.; Johnson, M.; Lee, F.; Nilakantan, R.; Petersen, R.; Svenson, K.; Chopra, R.; Tam, M. S.; Wen, Y.; Ellingboe, J.; Arndt, K.; Boschelli, F. Discovery of benzisoxazoles as potent inhibitors of chaperone heat shock protein 90. *J. Med. Chem.* **2008**, *51*, 373–375.
- (57) Kung, P. P.; Funk, L.; Meng, J.; Collins, M.; Zhou, J. Z.; Johnson, M. C.; Ekker, A.; Wang, J.; Mehta, P.; Yin, M. J.; Rodgers, C.; Davies, J. F.; Bayman, E.; Smeal, T.; Maegley, K. A.; Gehring, M. R. Dihydroxyphenyl amides as inhibitors of the Hsp90 molecular chaperone. *Bioorg. Med. Chem. Lett.* **2008**, *18*, 6273–6278.
- (58) Kung, P. P.; Huang, B.; Zhang, G.; Zhou, J. Z.; Wang, J.; Digits, J. A.; Skaptason, J.; Yamazaki, S.; Neul, D.; Zientek, M.; Elleraas, J.; Mehta, P.; Yin, M. J.; Hickey, M. J.; Gajiwala, K. S.; Rodgers, C.; Davies, J. F.; Gehring, M. R. Dihydroxyphenylisoindoline amides as orally bioavailable inhibitors of the heat shock protein 90 (Hsp90) molecular chaperone. *J. Med. Chem.* **2010**, *53*, 499–503.
- (59) Chessari, G.; Congreve, M.; Figueroa, E.; Frederickson, M.; Murray, C. W.; Woolford, A. J.; Carr, M. G.; O'Brien, M. A.; Woodhead, A. J. Preparation of Benzamides as Hsp90 Inhibitors. WO2006109075, 2006.
- (60) Chessari, G.; Congreve, M.; Figueroa, E.; Frederickson, M.; Murray, C. W.; Woolford, A. J.; Carr, M. G.; Downham, R.; O'Brien, M. A.; Phillips, T. R.; Woodhead, A. J. Preparation of Hydroxybenzamides as Hsp90 Inhibitors. WO2006109085, 2006.
- (61) Funk, L. A.; Johnson, M. C.; Kung, P. P.; Meng, J. J.; Zhou, J. Z. Preparation of Hydroxyarylcarboxamide Derivatives for Treating Cancer. WO2006117669, 2006.
- (62) Verdonk, M. L.; Rees, D. C. Group efficiency: a guideline for hits-to-leads chemistry. *ChemMedChem* **2008**, *3*, 1179–1180.
- (63) Taber, D. F.; Korsmeyer, R. W. Simple stereoselective synthesis of (±)-oplopanone. *J. Org. Chem.* **1978**, *43*, 4925–4927.
- (64) Mutsukado, M.; Tanikawa, K.; Shikada, K.; Sakoda, R. 3(2H)-Pyridazinones and Antiallergic Agents Containing Them. EP193853, **1986**.
- (65) Dalvit, C.; Pevarello, P.; Tato, M.; Veronesi, M.; Vulpetti, A.; Sundstrom, M. Identification of compounds with binding affinity to proteins via magnetization transfer from bulk water. *J. Biomol. NMR* **2000**, *18*, 65–68.
- (66) Leslie, A. G. W.; Brick, P.; Wonacott, A. MOSFLM. *Daresbury Lab. Inf. Q. Protein Crystallogr.* **2004**, *18*, 33–39.
- (67) Collaborative Computational Project, No. 4. The CCP4 suite: programs for protein crystallography. *Acta Crystallogr.* **1994**, *D50*, 760–763.
- (68) Stebbins, C. E.; Russo, A. A.; Schneider, C.; Rosen, N.; Hartl, F. U.; Pavletich, N. P. Crystal structure of an Hsp90-geldanamycin complex: targeting of a protein chaperone by an antitumor agent. *Cell* **1997**, *89*, 239–250.
- (69) Obermann, W. M.; Sondermann, H.; Russo, A. A.; Pavletich, N. P.; Hartl, F. U. In vivo function of Hsp90 is dependent on ATP binding and ATP hydrolysis. *J. Cell Biol.* **1998**, *143*, 901–910.
- (70) Murshudov, G. N.; Vagin, A. A.; Dodson, E. J. Refinement of macromolecular structures by the maximum-likelihood method. *Acta Crystallogr. D* **2004**, *D53*, 240–255.
- (71) Roversi, P.; Blanc, E.; Vonnrhein, C.; Evans, G.; Bricogne, G. Modelling prior distributions of atoms for macromolecular refinement and completion. *Acta Crystallogr., Sect. D: Biol. Crystallogr.* **2000**, *56*, 1316–1323.
- (72) Mooij, W. T.; Hartshorn, M. J.; Tickle, I. J.; Sharff, A. J.; Verdonk, M. L.; Jhoti, H. Automated protein–ligand crystallography for structure-based drug design. *ChemMedChem* **2006**, *1*, 827–838.
- (73) Hartshorn, M. J. AstexViewer: a visualisation aid for structure-based drug design. *J. Comput.-Aided Mol. Des* **2002**, *16*, 871–881.
- (74) Emsley, P.; Cowtan, K. Coot: model-building tools for molecular graphics. *Acta Crystallogr., Sect. D: Biol. Crystallogr.* **2004**, *60*, 2126–2132.
- (75) Laskowski, R. A. PDBsum: summaries and analyses of PDB structures. *Nucleic Acids Res.* **2001**, *29*, 221–222.
- (76) Turnbull, W. B.; Daranas, A. H. On the value of *c*: can low affinity systems be studied by isothermal titration calorimetry? *J. Am. Chem. Soc.* **2003**, *125*, 14859–14866.
- (77) Onuoha, S. C.; Mukund, S. R.; Coulstock, E. T.; Sengerova, B.; Shaw, J.; McLaughlin, S. H.; Jackson, S. E. Mechanistic studies on Hsp90 inhibition by ansamycin derivatives. *J. Mol. Biol.* **2007**, *372*, 287–297.
- (78) Sigurskjold, B. W. Exact analysis of competition ligand binding by displacement isothermal titration calorimetry. *Anal. Biochem.* **2000**, *277*, 260–266.
- (79) Shao, Y.; Molnar, L. F.; Jung, Y.; Kussmann, J.; Ochsenfeld, C.; Brown, S. T.; Gilbert, A. T.; Slipchenko, L. V.; Levchenko, S. V.; O'Neill, D. P.; DiStasio, R. A., Jr.; Lochan, R. C.; Wang, T.; Beran, G. J.; Besley, N. A.; Herbert, J. M.; Lin, C. Y.; Van Voorhis, T.; Chien, S. H.; Sodt, A.; Steele, R. P.; Rassolov, V. A.; Maslen, P. E.; Korambath, P. P.; Adamson, R. D.; Austin, B.; Baker, J.; Byrd, E. F.; Dachsels, H.; Doerksen, R. J.; Dreuw, A.; Dunietz, B. D.; Dutoi, A. D.; Furlani, T. R.; Gwaltney, S. R.; Heyden, A.; Hirata, S.; Hsu, C. P.; Kedziora, G.; Khallilulin, R. Z.; Klunzinger, P.; Lee, A. M.; Lee, M. S.; Liang, W.; Lotan, I.; Nair, N.; Peters, B.; Proynov, E. I.; Pieniazek, P. A.; Rhee, Y. M.; Ritchie, J.; Rosta, E.; Sherrill, C. D.; Simmonett, A. C.; Subotnik, J. E.; Woodcock, H. L., III; Zhang, W.; Bell, A. T.; Chakraborty, A. K.; Chipman, D. M.; Keil, F. J.; Warshel, A.; Hehre, W. J.; Schaefer, H. F., III; Kong, J.; Krylov, A. I.; Gill, P. M.; Head-Gordon, M. Advances in methods and algorithms in a modern quantum chemistry program package. *Phys. Chem. Chem. Phys.* **2006**, *8*, 3172–3191.
- (80) Verdonk, M. L.; Chessari, G.; Cole, J. C.; Hartshorn, M. J.; Murray, C. W.; Nissink, J. W.; Taylor, R. D.; Taylor, R. Modeling water molecules in protein–ligand docking using GOLD. *J. Med. Chem.* **2005**, *48*, 6504–6515.
- (81) Watson, P.; Verdonk, M. L.; Hartshorn, M. J. A Web-based platform for virtual screening. *J. Mol. Graph. Modell.* **2003**, *22*, 71–82.
- (82) Jones, G.; Willett, P.; Glen, R. C. Molecular recognition of receptor sites using a genetic algorithm with a description of desolvation. *J. Mol. Biol.* **1995**, *245*, 43–53.
- (83) Eldridge, M. D.; Murray, C. W.; Auton, T. R.; Paolini, G. V.; Mee, R. P. Empirical scoring functions. 1. The development of a fast empirical scoring function to estimate the binding affinity of ligands in receptor complexes. *J. Comput.-Aided Mol. Des.* **1997**, *11*, 425–445.
- (84) Verdonk, M. L.; Cole, J. C.; Hartshorn, M.; Murray, C. W.; Taylor, R. D. Improved protein–ligand docking using GOLD. *Proteins* **2003**, *52*, 609–623.
- (85) Squires, M. S.; Feltell, R. E.; Wallis, N. G.; Lewis, E. J.; Smith, D. M.; Cross, D. M.; Lyons, J. F.; Thompson, N. T. Biological characterization of AT7519, a small-molecule inhibitor of cyclin-dependent kinases, in human tumor cell lines. *Mol. Cancer Ther.* **2009**, *8*, 324–332.